

**University of Göttingen**



Faculty of Geoscience and Geography  
Department of Structural Geology and Geodynamics

Bachelor Thesis

**How clay layers control basin-scale fluid and heat  
flow**

Author: Virginia Attje Ingrid Albertine Potter van Loon (21340509)  
Programme: Ecosystem Management  
Semester: Spring semester 2016  
First supervisor: Dr. Elco Luijendijk  
Second supervisor: Dr. Tom Gleeson  
Submission date: 16/06/2016

## Abstract

Previous research has demonstrated that groundwater flow influences temperatures in sedimentary basins. Low-permeability layers like clays have been shown to control fluid flow in watersheds. However, the role of clay layers has never been explored systematically. Therefore, the influence of different permeability scenarios on basin-scale flow remains disputed. This study focuses on clay layers in sedimentary basins, as extremes for a low permeability situation. From a newly compiled dataset, we conclude that marine shale layers are present in all of North America and roughly 40% of the research area in Europe. We use numerical models to compare clay with no clay scenarios, for the range of watersheds found in the dataset. Furthermore, we explore the effects of clay layer thickness, depth and mineralogy on fluid and heat flow. Base case scenario results show that a shale layer reduces vertical fluid flow to below 1 cm/yr and decreases the cooling effect of recharge by up to 20 °C. Due to the presence of a clay layer, the flow velocity and temperature deviation increases with increasing hydraulic gradient and declining clay content of the sediment surrounding the clay layer. A shale layer blocks vertical fluid flow regardless of basin dimension. Vertical fluid flow velocity decreases with increasing dimension for clay layer free watersheds. The recharge cooling effect is strongest when the basin half-length equals approximately 50 km. We also conclude that all clay layers in our dataset block fluid flow. As clay layer thickness increases, flow velocity and temperature change decline. Moreover, we find that continuous kaolinite, illite and smectite layers of 10 – 100 m, 1-10 cm and 0.1-1.0 mm thick respectively, block groundwater flow. Moreover, we find that the suppression of heat flow decreases with clay layers burial depth, allowing a cooling effect up to -11 °C.

# Table of Contents

<b>1 Introduction .....</b>	<b>1</b>
<b>2 Method .....</b>	<b>3</b>
<b>2.1 Data set compilation.....</b>	<b>3</b>
<b>2.2 Model code .....</b>	<b>4</b>
<b>3 Results .....</b>	<b>9</b>
<b>3.1 The effect of a clay layer .....</b>	<b>9</b>
<b>3.2 The effect of a clay layers in different basins.....</b>	<b>10</b>
3.2.1 Fluid flow .....	11
3.2.2 Heat flow .....	14
<b>3.3 The effect of different clay layers .....</b>	<b>17</b>
3.3.1 Fluid flow .....	17
3.3.2 Heat flow .....	20
<b>4 Discussion .....</b>	<b>23</b>
<b>4.1 Results literature comparison .....</b>	<b>23</b>
<b>4.2 Limitations and implications .....</b>	<b>23</b>
<b>5 Conclusion .....</b>	<b>26</b>
<b>6 Acknowledgement .....</b>	<b>28</b>
<b>7 Literature.....</b>	<b>29</b>
<b>8 Appendix .....</b>	<b>33</b>
<b>Appendix A.....</b>	<b>33</b>
1.1 Fluid flow .....	33
1.2 Fluid viscosity and density .....	34
1.3 Permeability .....	34
1.4 Porosity .....	37
1.5 Heat Flow .....	37
<b>Appendix B – E .....</b>	<b>39</b>

# 1 Introduction

Previous research has shown that ground water flow affects heat flow in the subsurface, accounting for several tens of degrees of temperature difference with respect to model not incorporating its effects (Kooi, 2015; Deming, 1994; Anderson, 2005).

The effect of groundwater flow on temperature is clearly influenced by the permeability of the different sediments. Low permeability sediments such as clay, obstruct the water from flowing downwards, compared to highly permeable sediments such as sand. By obstructing or allowing recharge to reach deeper sections of the basin also heat flow is affected. Here again, clay hinders recharge to function as a cooling agent, compared to sand (Neuzil, 1986; Bjørlykke et al. 1988).

Although ample has been published on the effect of basin scale fluid flow on heat flow (Kooi, 2005; Deming, 1994; Anderson, 2005), little research has been done on the role that low permeability sediments, especially clay, plays in this process. Consequently, the role of ground water flow on subsurface temperature remains disputed (Anderson, 2005; Corbet and Bethke, 1992). Bjørlykke et al. (1988) show that a thin, low permeability layer ( $< 1\text{m}$ ) splits a thermal convection cell into two functional smaller cells, thereby demonstrating that permeability can strongly alter the fluid and heat flow in a basin. By neglecting to take permeability into account it is likely that regional fluid flow is misestimated. Also, heat flow inventories will be affected, by over or underestimating the local temperatures or geothermal gradients.

By unraveling how clay layers control fluid and heat flow, reconstructions of the subsurface can be simulated with higher accuracy. Elaborate knowledge of the dimensions can find application in for instance nuclear waste research and initiatives. Shale formations are considered attractive hosts for nuclear

and other hazardous waste due to their low permeability and high sorption capacity. Knowledge on the hydrology in these layers is key in order to predict to what extent they can isolate contaminants (Hendry, 2015). Also, economic viability of geothermal wells depends on permeability and heat flow i.e. geothermal gradient values. More in depth knowledge of the effects of a low permeability zone can accelerate and reduce costs of for example site inventories (Barbier, 2002). Moreover, hydrocarbon resources are directly related to heat flow, with high geothermal gradients resulting in above average reserves (Klemme, 1972).

This study investigates how clay layers affect fluid and heat flow in terrestrial sedimentary basins. First, we present a new database, compiling information on the properties of sedimentary basins, watershed characteristics and clay layer information. Then, we introduce a conceptual model, which forms the base for the sensitivity analysis. Next, follows the sensitivity analysis, in which we first compare simulations containing clay with non-clay scenarios. Second, we reconstruct groundwater and heat flow for a range of basins with and without a clay layer, by varying the basin dimension, hydraulic gradient and clay content in the sediment surrounding the shale zone. Last, we simulate various shale layer depth and thickness scenarios. All three parts of the sensitivity analysis are done, using a numerical finite element model of fluid and heat flow. With this numerical approach, regional fluid and heat flow is reconstructed in a 2D cross section. The chief software used is a customized version of SUTRA by the USGS. The model operates in steady state conditions.

## 2 Method

This chapter will elaborate on the approach used in this study to determine how clay layers control fluid and heat flow in sedimentary basins.

### 2.1 Data set compilation

We compiled a new GIS database for this study containing information on watersheds in North America and Europe. For both continents a sedimentary basin and hydroshed polygon dataset were intersected. The sedimentary basin set originates from research conducted by Gleeson et al. (2016) and narrowed our database down to sedimentary basins. The hydroshed data set obtained from Lehner et al. (2006) contains information on river distance and hydraulic gradient.

For North America we used a point GIS dataset containing information on shale layer depth and thickness obtained from Macrostrat ([www.macrostrat.org](http://www.macrostrat.org)). Each polygon of the aforementioned merger obtained the value of the data point closest to its gravitational center.

The data on clay layer thickness and depth in Europe bases on TNO map material (Doornbal et al., 2010). We digitized quaternary and tertiary base depth maps, as well as thickness maps for the late Paleocene, Eocene, Oligocene and Miocene. Also, we digitized maps identifying the location of marine shale layers in the Rupelian. We determined shale zone thickness and depth by stacking the different Cenozoic maps and comparing them to thickness tertiary and quaternary maps. The results were interpolated to smooth out the coarse transition values due to the maps' gross scale.

Results from the data compilation show that a marine clay layer covers all of North America. 40 % of sedimentary basins of the mapped area in Europa contain marine clay layers. According to the dataset the median values for

river distance, clay layer thickness, clay layer depth and hydraulic gradient are 9240.8 m, 20.6 m, 171.4 m and 1.7232 % respectively. The distribution curve for the abovementioned parameters is presented in Figure 1.

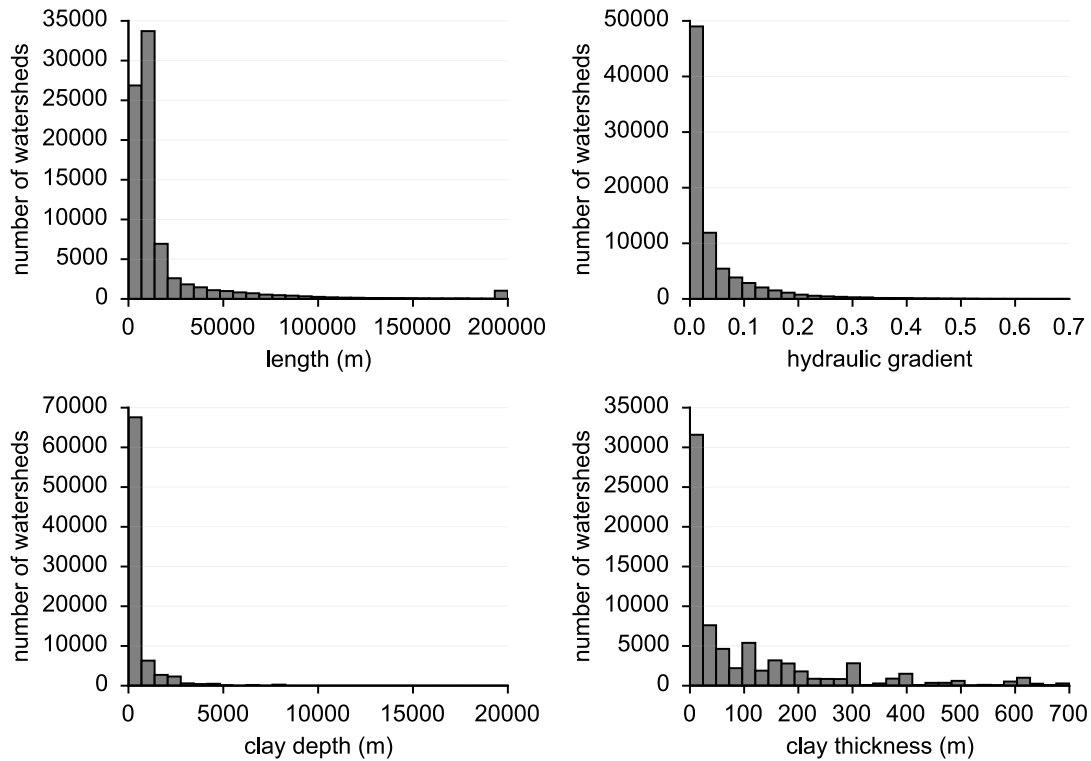


**Figure 1.** Distribution curve for river distance (m), hydraulic gradient, clay layer depth (m) and clay layer thickness (m)

## 2.2 Model code

The model code simulates the relation between clay layers and fluid and heat flow in sedimentary basins, because they tend to “layer” horizontally with relatively few complex constructions (Allen & Allen, 2005). Only sedimentary basins that are currently on land are taken into account. The model assumes steady state and saturated conditions. The grid resolution equals 200 cells in the x-direction and 150 cells in the y-direction.

The fluid and heat flow equations (Appendix A) were solved iteratively by a numerical finite element code, SUTRA (Vos and Prevost, 2010). Base case

parameter values and parameter value range are presented in table 1. Values of constants used in all simulations are presented in table 2. All fluid flow is assumed to be fresh water, thereby neglecting any salinity affects.

**Table 1.** Base case parameter values and parameter value range

Parameter	Base case value	Variation range for sensitivity analysis
River distance	9240.8 m	3.029 km – 200 km
Hydraulic gradient	0.017232	$2.175e^{-3}$ – 0.18
Clay content of the sediment surrounding the clay layer	0.1	0.0 – 0.55
Clay layer thickness	20.6 m	4 – 299.3 m and $1e^{-5}$ – 100 m
Clay layer depth	171.4 m	5 – 1658 m

**Table 2.** Values of constants used in all simulations

Parameter	Value	Source
Gravity ( $ms^{-2}$ )	9.81	
Composition clay layer	50% Kaolinite, 50% Illite	Luijendijk et al. (2015)
Permeability ( $m^2$ )		Luijendijk et al. (2015)
Kaolinite	$6.16e^{-17}$	
Illite	$1.54e^{-19}$	
Smectite	$1.18e^{-21}$	
Specific surface per volume of solid grain ( $m^{-1}$ )	$181e^3$	See Appendix A
Empirical clay permeability parameter		Luijendijk et al. (2015)
Kaolinite	3.61	

Illite	3.58	
Smectite	3.01	
Basal heat flow ( $\text{Wm}^{-2}$ )	65	Davies (2013)
Surface temperature ( $^{\circ}\text{C}$ )	10	Hansen et al. (1999)
Anisotropy	10	Luijendijk et al. (2015)
Power mean efficient	0	Luijendijk et al. (2015)
Porosity-depth parameter ( $\text{m}^{-1}$ )	$4 - 9 \text{ e}^{-4}$	Luijendijk (2012)
Thermal conductivity ( $\text{Wm}^{-1}\text{K}^{-1}$ )	2.5	Allen et al. (2005)
Solids	0.6	
Liquids		

The model reconstructs a 2D cross-section governed by saturated and steady state conditions. The cross section stands perpendicular on the discharge point, such as a river or lake. The conceptual models for fluid and heat flow are presented in figure 2. The model reconstructs 4 horizontal layers. The lowest one shown in figure 2 in dark gray represents crystalline rock. The light gray layer represents the clay layer. The surrounding white layers are coarse sediments.

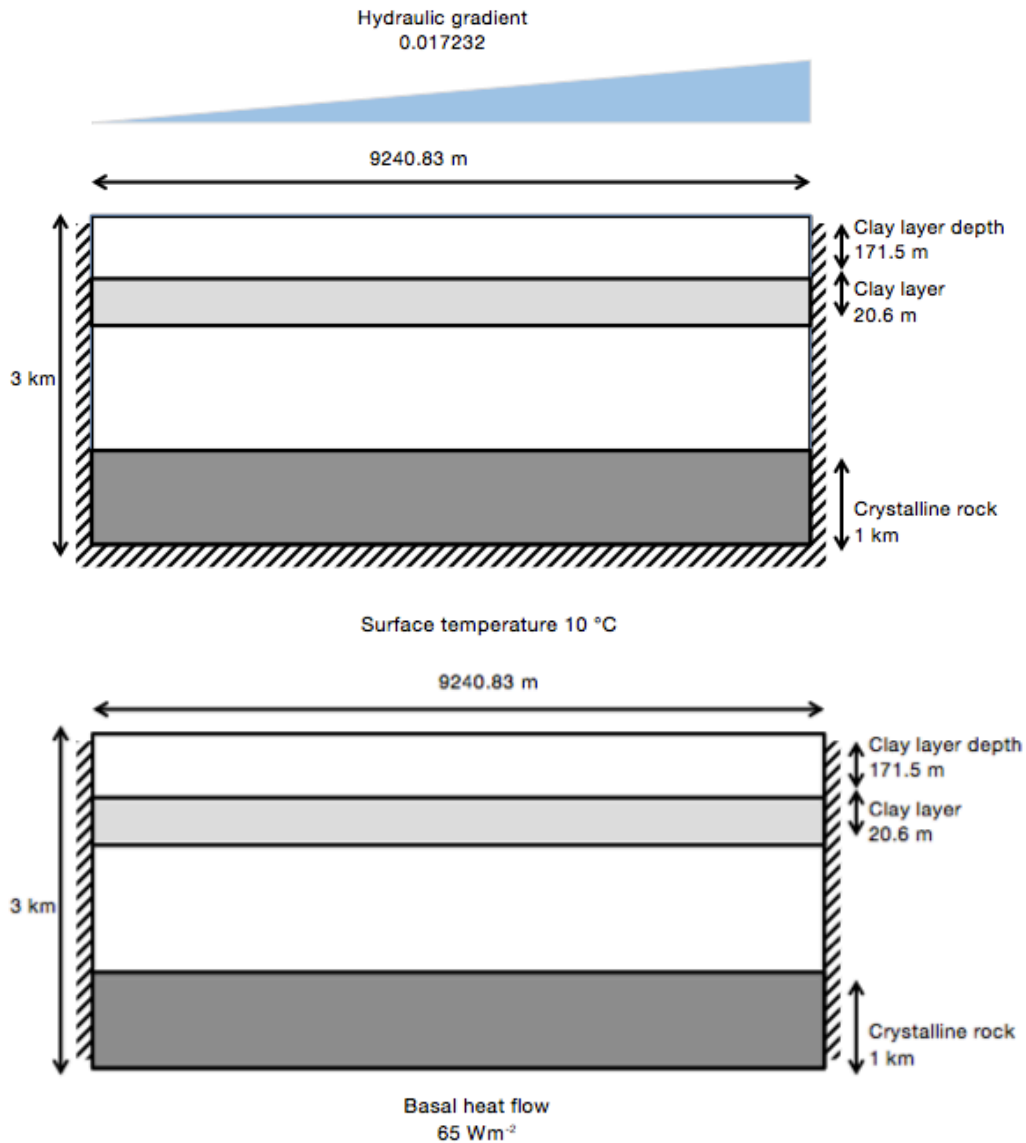


**Figure 2.** Conceptual models for fluid flow (above) and heat flow (below) with base case values. The dark and light gray layers represent the clay and crystalline rock zone, respectively. The white layers illustrate the surrounding coarse sediment.

For fluid flow, there are no flow boundaries at the sides and at the bottom of the model. Moreover, the hydraulic gradient is specified, thereby it allows flux i.e. recharge and discharge to occur. Consequently, the discharge recharge boundary is located roughly in the middle of the cross section. The hydraulic gradient leaves the left end in figure 2 to function as a discharge center such as a river or lake. The 2D cross section stands perpendicular on this river, as mentioned afore. Permeability is assumed to follow Lujendijk et al. 2015.

Boundary conditions for the heat flow simulation differ slightly. There are no heat flow boundaries on both sides of the model. The bottom is governed by a specified basal heat flow of  $65 \text{ Wm}^{-2}$ . Temperature at the top is also specified and equals the surface temperature, which is  $10 \text{ }^{\circ}\text{C}$ . In the results all temperature related figures present the difference between a flow and no flow scenario. We chose temperature change instead of actual temperature, because it allows clearer visualization of relatively small temperature differences.

As seen from in table 2, the clay layer is assumed to be a mixture of 50% kaolinite and 50% illite. The surrounding sediments are assignment a clay fraction of 10%, which is an adjusted value in order to achieve a realistic permeability of approximately  $5 \times 10^{-14} \text{ m}^2$  (Gleeson et al., 2011).

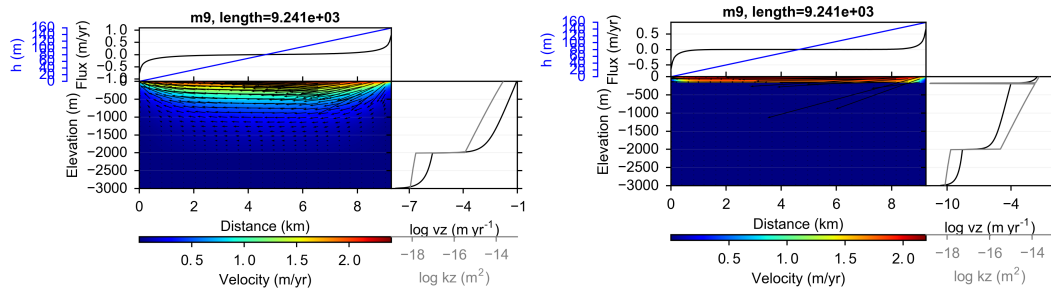
Table 1 presents the base case values and the parameter value range used in the sensitivity analysis. All values originate from our newly compiled database, which we use to reconstruct what happens in nature i.e. existing basins. First, we explore the effect of a clay layer in a “median” or base case scenario. Second, we reconstruct a base case clay layer in various watersheds and compare it to equivalent clay layer free scenarios. We test the following watershed parameters: basin dimension, hydraulic head and the clay content of the surrounding sediment. Hereby, we try to see how strongly a clay layer changes mean fluid and heat flow in different sedimentary basins. Also, we explore how above, below and in clay layer vertical flow velocity and temperature change alters with varying basin properties. Last, we vary the characteristics of clay layers in base case basins to identify how strongly clay layer properties influence basin-scale fluid and heat flow. We vary clay layer depth and clay layer thickness. Also, we test at what thickness pure, continuous kaolinite, illite and smectite layers and the kaolinite illite mix layer mentioned before reduce vertical flow velocity in the clay layer to below  $1 \text{ cm/yr}$ .

### **3 Results**

The results of the sensitivity analysis are divided into three parts, which all analyze the effect of clay layers on fluid and heat flow from different perspectives. The first, compares base case value watershed with a clay layer to one without. Hereby, it demonstrates the general effect of a clay layer on basin-scale fluid and heat flow. The second part, demonstrates the effects of the shale zone on a range of watersheds by varying dimension, hydraulic gradients and the clay fraction in the surrounding sediment. The third part fluctuates the depth and thickness of the shale layer.

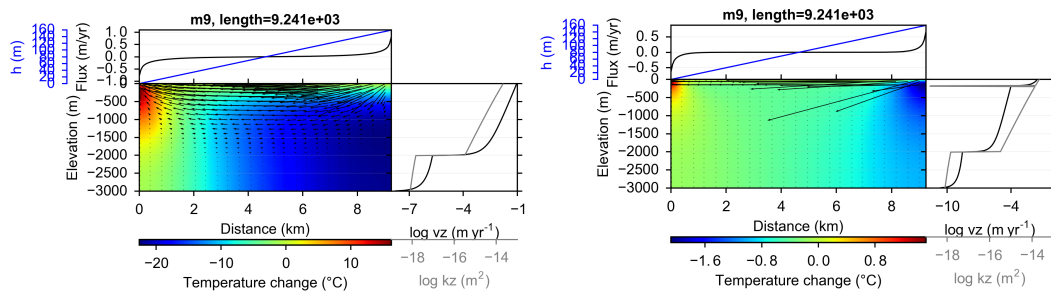
#### **3.1 The effect of a clay layer**

Figure 3 demonstrates fluid flow indicated by vertical flow velocity for a base case with and without a clay layer. The clay layer is approximately 20 m thick and buried roughly 170 m deep. Basin dimension, hydraulic gradient and clay content assume approximately 9 km, 1.7 % and 10 %, respectively. The dark grey line in the right panel and the colors in the 2D cross section show the vertical flow velocity. In the no clay scenario the flow velocity decreases much slower with depth than in its counter part with shale. Also, in the basin representations themselves higher velocities persist deeper when there is no clay and diminish abruptly around the crystalline rock zone. In the clay layer free scenario, groundwater submerges around the recharge center (at the flux maximum), moves horizontally in the middle of the basin and arises at the flux minimum, where most discharge takes place. Additionally, in the clay layer free basin, velocity approaches 0 m/yr around 2 km depth where the crystalline rock basement commences. When integrating a clay layer, flow velocity equal approximately 0 m/yr from the shale zone downwards.



**Figure 3.** Vertical flow velocity (m/yr) for a base case without clay layer (left) and with clay layer (right)

The temperature change, shown in figure 4, is the difference between a flow and no-flow scenario. All other parameters assume the base case values of mentioned afore. Without the clay layer, temperature change values range from -20 °C to + 10 °C. With a non-permeable zone the temperature scope decreases to - 2 °C to + 1 °C. Cooling primarily takes place around the flux maximum i.e. recharge maximum, whilst heating is centered around the flux minimum, i.e. discharge location. The temperature change is barely affected by the transition to the crystalline rock basement at 2 km depth.



**Figure 4.** Temperature change (°C) for a base case without clay layer (left) and with clay layer (right)

### 3.2 The effect of a clay layers in different basins

This section elaborates on the effect of clay layer on fluid and heat flow in different basins. We reconstruct watersheds with varying basin dimension, hydraulic gradient and clay content. We obtained the value range for the first

two parameters from a newly compiled database (see 2.3). Clay content was estimated as described in subsection 2.3.

### 3.2.1 Fluid flow

The influence of basin dimension on fluid flow in the cross section is illustrated in the two scenarios in figure 5. The first demonstrates a setting in which the half-length equals roughly 3 km. The clay layer is represented in the grey logarithmic permeability graph right of the figure at roughly 170 m depth. Above the blockage, velocity is highest in the middle of the basin and decreasing towards both left and right. This pattern does not apply to the second scenario in figure 5, which is identical, except for the river distance, which here equals 200 km. In the longer basin there is a significant flow velocity below the shale layer, with values up to 0.5 m/yr. Below and in the clay layer vertical flow velocity is a logarithmic factor two higher in the bigger basin, as indicated by the dark grey velocity curve. The velocity decreases with depth and approaches zero around the crystalline rock basement. From the clay layer upward the majority of the basin experiences velocities around 1.5 to 2 m/yr. Above the clay layer flow velocity is higher in the larger basin. Around the flux maximum and minimum velocity decreases with depth.

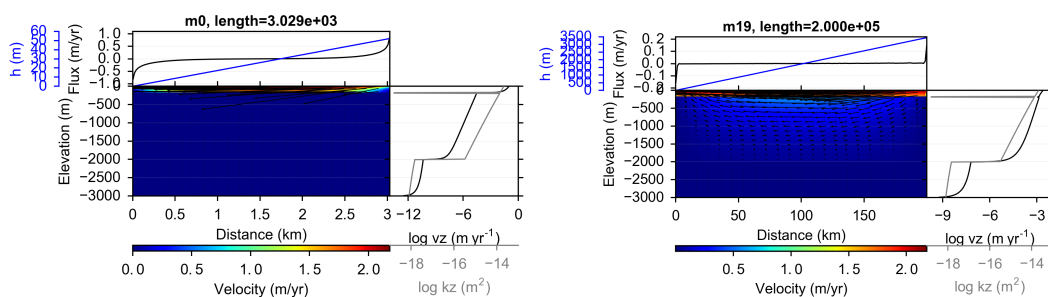


**Figure 5.** Vertical flow velocity (m/yr) for a river distance of 3.029 km (left) and a river distance of 200 km (right)

With increasing hydraulic gradient, above-clay layer velocity increases strongly (see figure 6). Fluid flows roughly 10 times faster with velocities up to 25 m/yr if the hydraulic slope equals 0.18, in comparison with a maximum to 0.28 m/yr for a hydraulic gradient of  $2/10^{-13}$ . As visible in the velocity

curve, the vertical flow velocity in and below the clay layer is a logarithmic factor two higher in the basin with the higher hydraulic gradient.

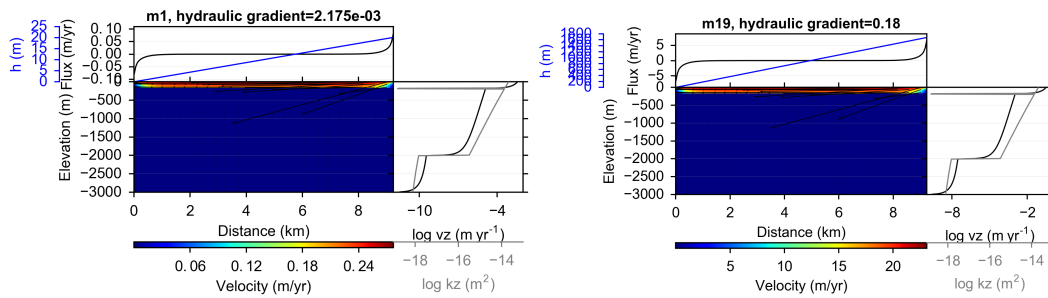


**Figure 6.** Vertical flow velocity (m/yr) for a hydraulic gradient of  $2.175e^{-3}$  (left) and a hydraulic gradient of 0.18 (right)

If the sediment that surrounds the shale zone contains no clay, flow velocity ranges from 0 to 10 m/yr (see figure 7). When increasing the shale fraction to 55 % velocity merely ranges between 0.000 and 0.004 m/yr. In the latter a flow pattern below the clay layer is visible, whilst no movement can be identified in the 0 % clay fraction scenario. The flow follows a downward movement around the recharge maximum, followed by a horizontal migration that ascend when approaching discharge. The dark grey curve shows that the vertical flow velocity is lower in the right figure for all layers, expect for the crystalline rock. The light grey curve for the right scenario demonstrates that with depth, the sediment with a clay fraction of 55% becomes less permeable than the underlying crystalline rock basement. The velocity curve shows how the effect of the clay layer on flow velocity decreases with increasing clay content.

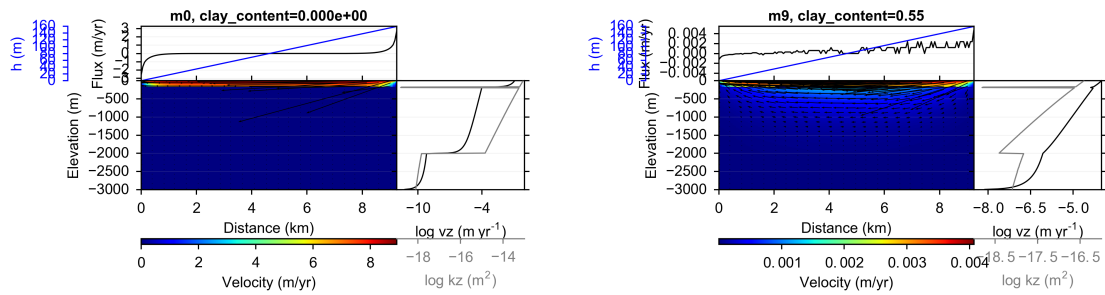


**Figure 7.** Vertical flow velocity (m/yr) for in the clay layer for a surrounding sediment with a clay content of 0% (left) and a clay content of 55% (right)

Figure 8 shows the results for all runs from the sensitivity analyses regarding basin characteristics and fluid flow. The vertical flow velocity in the clay layer represents the latter. For the clay free scenario, the velocity is determined for the same location i.e. a 20 m thick area at 170 m depth. As a general trend groundwater flow velocity decreases with declining basin dimensions in the clay free scenario. The majority of basins have a half-length of 25 km or less and in most cases flow velocity in the clay layer will be approximately 0 m/yr. In the equivalent non shale layer zone, velocity will be slightly above 0 m/yr.

Velocity increases as the hydraulic gradient becomes higher, for the clay layer free scenario. This effect is practically disabled by the clay layer (see figure 8). Most watersheds have a hydraulic gradient of 10 % or less and thereby velocities, attributed to this parameter ranging from 0 to 0.5 m/yr will be the most common.

Mean vertical flow velocity in the shale layer and its equivalent approaches 0 m/yr, regardless of the clay content of the surrounding sediment. Nevertheless, for the equivalent clay zone free scenario, layer velocity does decrease slightly as the clay fraction increases.

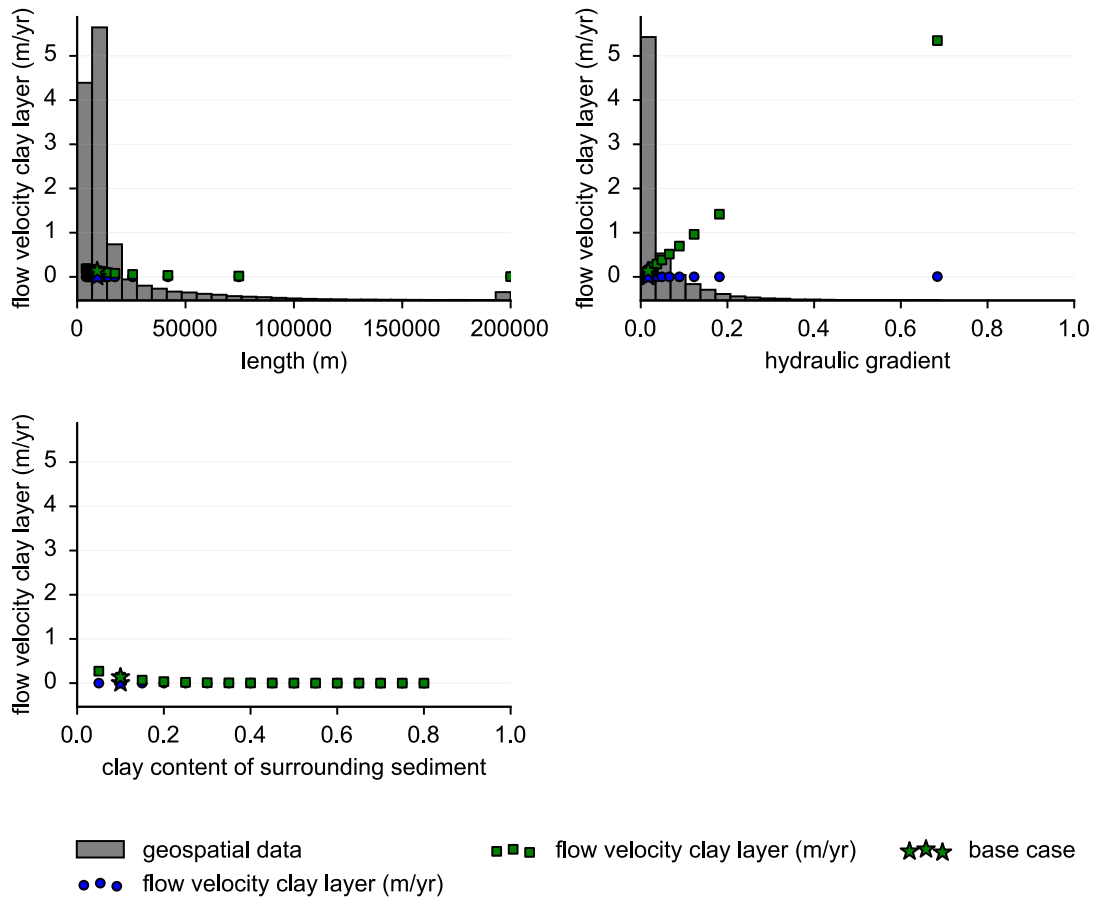


**Figure 8.** Flow velocity in the clay layer (m/yr) in the clay layer (circles) and in the same layer without any clay (squares) as function of river distance (left above), hydraulic gradient (right above) and clay content (below) with the probability distribution of the respective parameter presented in the histograms.

### 3.2.2 Heat flow

Figure 9 shows one of the smallest water shed dimensions present in the dataset, in which the river distance equals roughly 3 km. The right end area with the highest flux experiences a cooling effect of up to  $-2\text{ }^{\circ}\text{C}$ . At the discharge location, which is represented by the negative flux, temperature change is positive. The majority of the basin experiences a cooling effect in comparison to a no flow scenario. Also, in the crystalline rock the cooling effect persists. The temperature pattern differs when dimensions increase, as presented in figure 9. The range of temperature change diverges slightly from

the previous scenario with values between approximately - 3 and + 1.5 °C. However, the distribution is significantly different. A much bigger fraction of the basin is experiencing a warming effect, which unlike with the smaller dimension reaches far into the crystalline rock. Also the second scenario in figure 9 shows a much clearer flow pattern, following a downward direction on the right half and arising on the left i.e. discharge side.

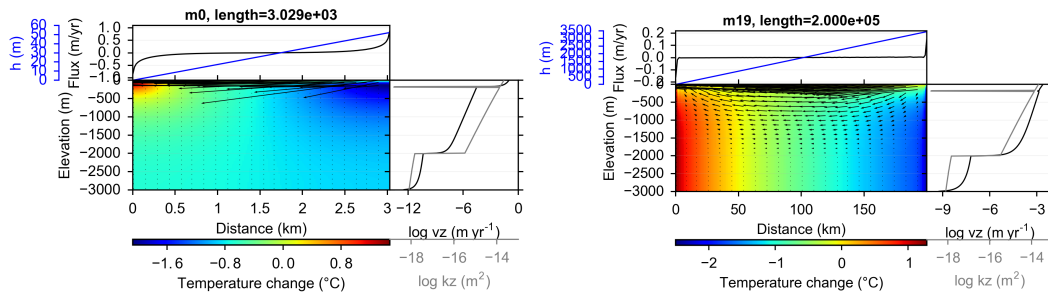


**Figure 9.** Temperature difference (°C) for a river distance of 3.029 km (left) and a river distance of 200 km (right)

As hydraulic head increases, the range of temperature change values expands from - 0.3 - + 0.15 °C to - 5 - + 1 °C (see figure 10). In the first scenario, a bigger fraction of the basin experiences a warming effect, whilst the latter is almost entirely subject to cooling. In both settings, a clear flow pattern is absent, indicating the disruption of groundwater movement due to the clay layer.

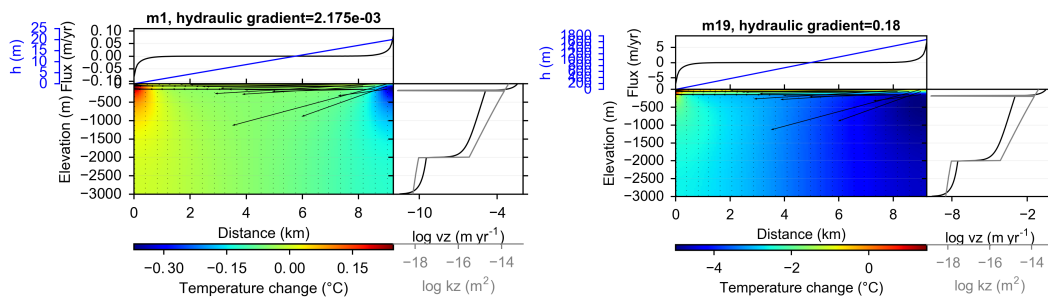


**Figure 10.** Temperature difference (°C) for a hydraulic gradient of 2.175e-3 (left) and a hydraulic gradient of 0.18 (right)

In figure 11 the range of temperature change decreases strongly as clay content increments. In the high clay fraction scenario, there seems to be a clearer division in the basin, which is heated in the left part and cooled in the right. However, the difference in value is relatively small. The clay free sediment scenario experiences heating only in a fraction of the basin, where discharge is concentrated.

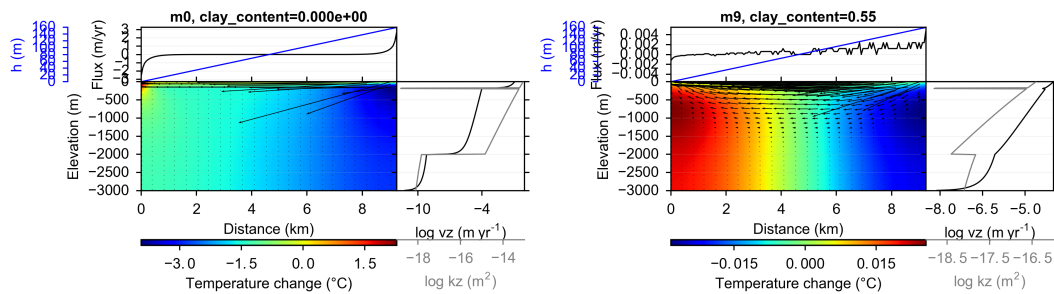


**Figure 11.** Temperature change (°C) for clay layer surrounding sediment with a clay content of 0% (left) and a clay content of 55% (right)

Figure 12 summarizes the results of the complete range of the sensitivity analysis. For basins with a shale layer temperature remains fairly constant as a function of river distance. Clay layer free basins experience a maximum around 10 km. Most river distance are 25 km or less. Thus, without clay the mean temperature change will most commonly equal -10 °C, with temperature change will lie between 0 and -1 °C.

As the hydraulic gradient increases, the cooling effect of groundwater becomes stronger. Watershed with a clay layer, experience less cooling than clay layer free basins. Most basins have a hydraulic gradient of 5% or less, leaving most prevalent temperature change ranging from 0 to -2 °C for watersheds with a clay layer and 0 to -20 °C for those without.

Temperature change decreases with increasing clay fraction in the sediment surrounding the shale zone. This effect is stronger for basins that have no clay layer.

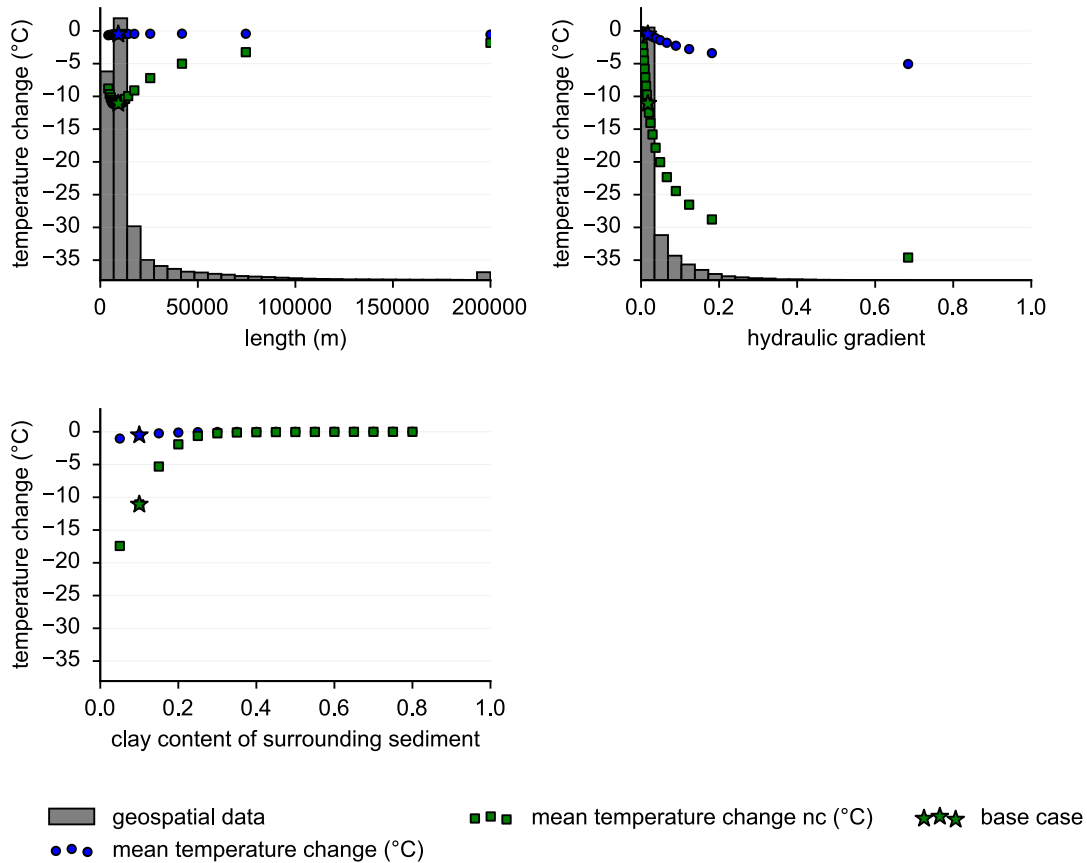


**Figure 12.** Mean temperature change (°C), in comparison to a no-flow scenario with a clay layer (circles) and without (squares) as function of river distance (left above), hydraulic gradient (right above) and clay content (below), with the probability distribution of the respective parameter presented in the histograms.

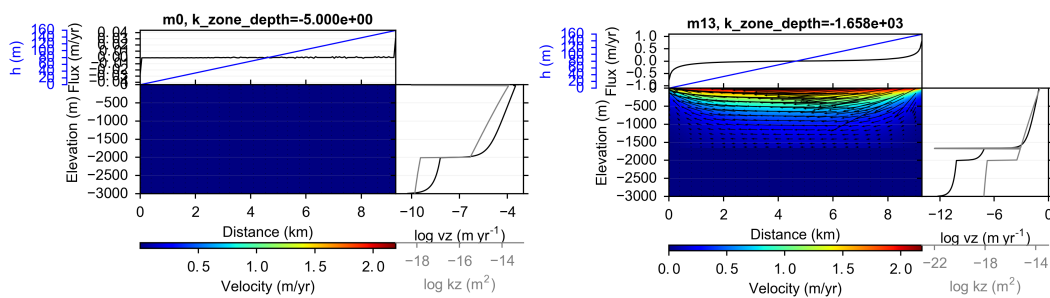
### 3.3 The effect of different clay layers

This chapter explores the effect of clay layer properties i.e. clay layer depth and thickness on basin-scale fluid and heat flow. The basin characteristics i.e. dimension, hydraulic head and clay content remain constant and assume median or estimated values.

#### 3.3.1 Fluid flow

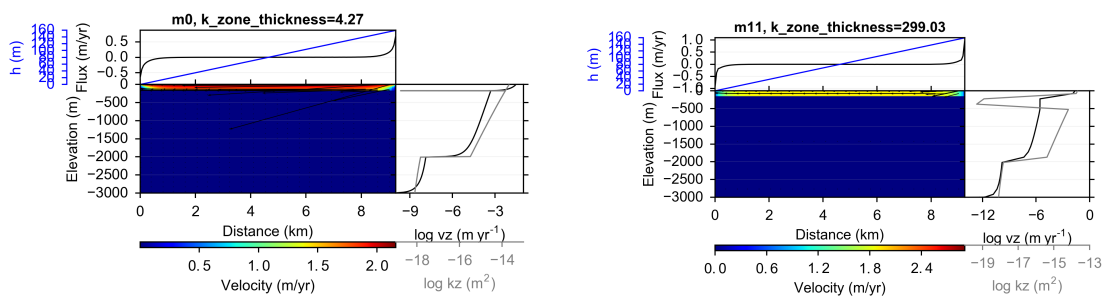
The shallow scenario in figure 13 appears to have no fluid flow at all. The absence of groundwater flow is probably not completely the case, but merely difficult to see due to the figure's resolution. The deep shale layer scenario in figure 13 shows velocities between 0 and 2.5 m/yr above the shale layer.

Velocity decreases with depth and approaches 0 m/yr at the clay layer. Velocity is also demonstrated in the dark grey velocity curve. In the shallow scenario velocity at the top is relatively low, and decreases constantly until approaching the crystalline rock basement. In the deep layer burial scenario, flow velocity is relatively high at the top, decreases much slower and abruptly declines when reaching the clay layer. Below the deep clay layer, flow velocity again reduces when approaching the crystalline rock basement. Overall, the velocity is lower in and below the clay layer and is higher above the clay layer for the deeper buried shale zone. In the latter setting, the velocity at 3 km depth is lower than in the shallow shale layer reconstruction.



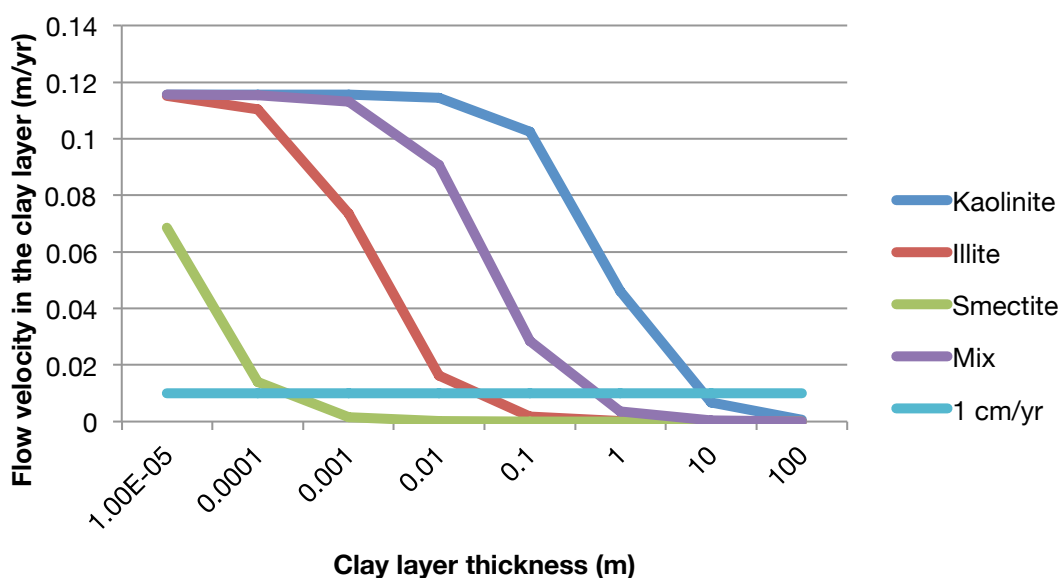
**Figure 13.** Vertical flow velocity (m/yr) for a 5 m deep clay layer (left) and a 1658 m deep clay layer (right)

Figure 14 demonstrates that both a 4 m and 299 m shale layer reduce vertical fluid flow, originating from recharge, to below 1 cm/yr. The dark gray curve demonstrates that velocity above the clay layer is higher for the thicker clay layer scenario, which is also visualized in the color panel. Vertical flow velocity is lower in and below the clay layer for the 299 m thick shale zone.



**Figure 14.** Vertical flow velocity (m/yr) for a 4 m thick clay layer (left) and a 299.03 m thick clay layer (right)

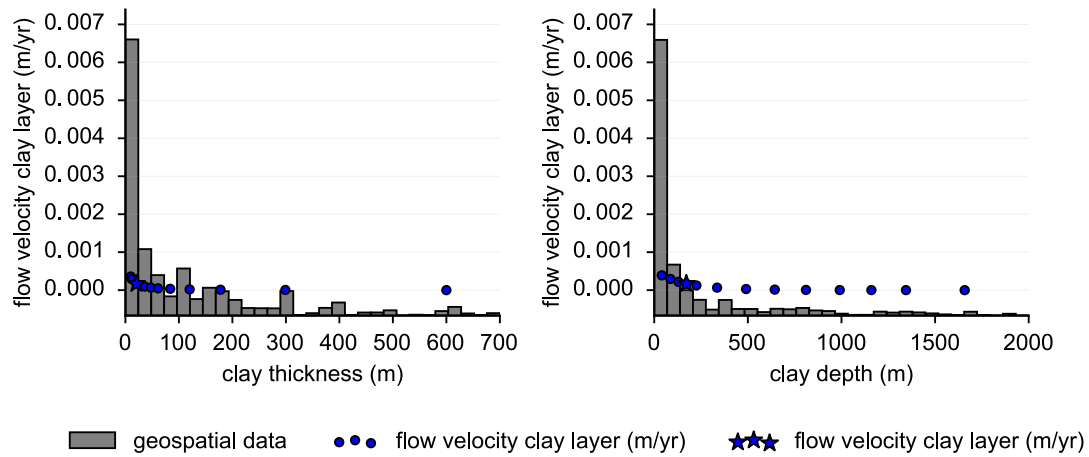
Seeing that the 4 m and 299 m thick clay layers are both comparably non-permeable, we also ran experiments with thinner clay layer scenarios to determine at what thickness a clay layer blocks fluid flow, i.e. reduces it to below 1 cm/yr. As mentioned earlier, the median clay layer was assumed to be a mixture to 50 % kaolinite and 50 % illite. The additional thickness runs address the kaolinite illite mix composition as well as pure kaolinite, illite and smectite. Results show that the kaolinite-illite cocktail becomes non-permeable between 10 cm and 1 m layer thickness. This border lies between 10 and 100 m, 1 and 10 cm and 0.1 and 1 mm, for pure kaolinite, illite and smectite, respectively (see figure 15).



**Figure 15.** Vertical flow velocity (m/yr) for kaolinite, illite, smectite, and mix clay layers as a function of shale layer thickness

Figure 16 summarizes the results of the tested value range. Vertical flow velocity in the clay decreases with its own thickness. Nevertheless, values are almost 0 for the smallest value i.e. 4 m thickness. Most basins have relatively thin clay layers between 4 and 50 m thick. Consequently, ground water velocity will slightly exceed 0 m/yr in the prevalent basin.

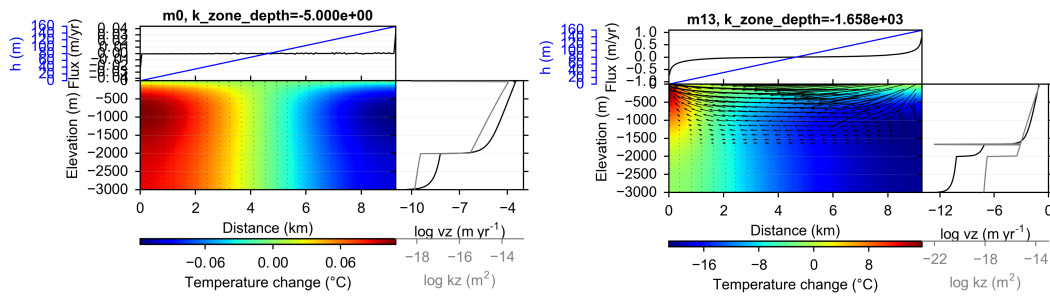
Flow velocity declines with clay layer burial depth. As the base case clay layer is 20 m thick, it functions a non-permeable zone, regardless of its location. Most shale zones lie at 100 m depth or less. However, due to the dimension of the clay layer, in shale velocity always approaches 0 m/yr.



**Figure 16.** Vertical flow velocity (m/yr) in the clay layer as function of clay layer thickness (left) and clay layer depth (right), with the probability distribution of the respective parameter presented in the histograms.

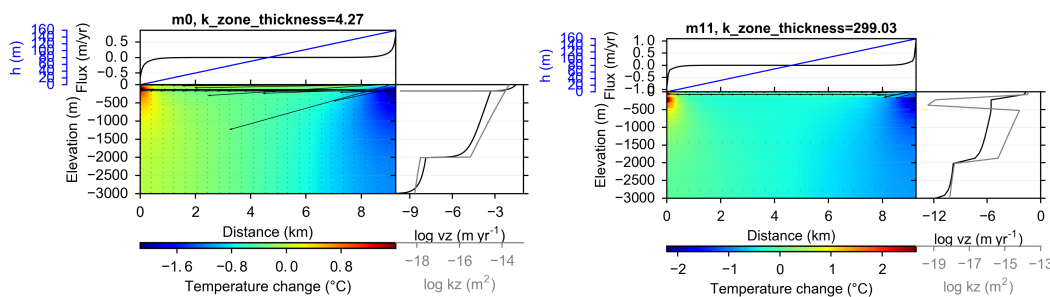
### 3.3.2 Heat flow

Figure 17 shows a scenario with a shale layer placed at 5 m depths. The positive and negative temperature changes are located at the flux maximum and minimum, respectively. The transition pattern of the shallow burial scenario differs strongly from its deep counterpart. The temperature differs from - 0.1 to + 0.1 °C. When locating the layer at - 1658 m depth, the temperature signature changes strongly. Temperature change ranges from - 20 °C to + 15 °C. A vast amount of the basin is cooled, there is no clear disruption of the temperature trend around the clay layer, even though it would be probable that a 20 m thick clay layers blocks fluid flow.



**Figure 17.** Temperature difference (°C) for a 5 m deep shale layer (left) and a 1658 m deep shale layer (right)

The thinnest shale layers in the database equal 4.27 m. Figure 18 shows a scenario with such a layer at median depth (-171 m). The cooling effect spreads from the max flux e.g. main recharge location, which is located at the right end of the figure. The warming effect is concentrated around the discharge point, placed at the left. All horizontally in between the recharge and discharge maxima appears a transition zone. The cooling and warming effect spreads all the way down through the sediment and the basement. In this scenario, the temperature difference ranges roughly from - 2 to + 1.5 °C. When increasing the thickness to the maximum, the dataset value of 299.03 m this range remain comparable. As both thicknesses blocks fluid flow, the bulk heat transfer can be assigned to conduction.



**Figure 18.** Temperature difference (°C) for a 4.27 m thick shale layer (left) and a 299.03 m thick clay layer (right)

In sum, mean temperature change decreases slightly with increasing clay layer thickness. As the thinnest clay layer in our dataset is 4 m thick, all shale zones in the sensitivity analysis function as fluid and heat flow barriers. Most

clay layers are no thicker than 50 m, leaving temperature change just below 0 °C.

Figure 19 also shows that temperature change increases as shale layers are buried deeper. When buried below 1500 m the effect reaches – 11 °C. Most clay zones are located on a relatively shallow level: between 5 and 100 m. Accordingly, the most prevalent temperature change ranges from 0 to -1 °C.

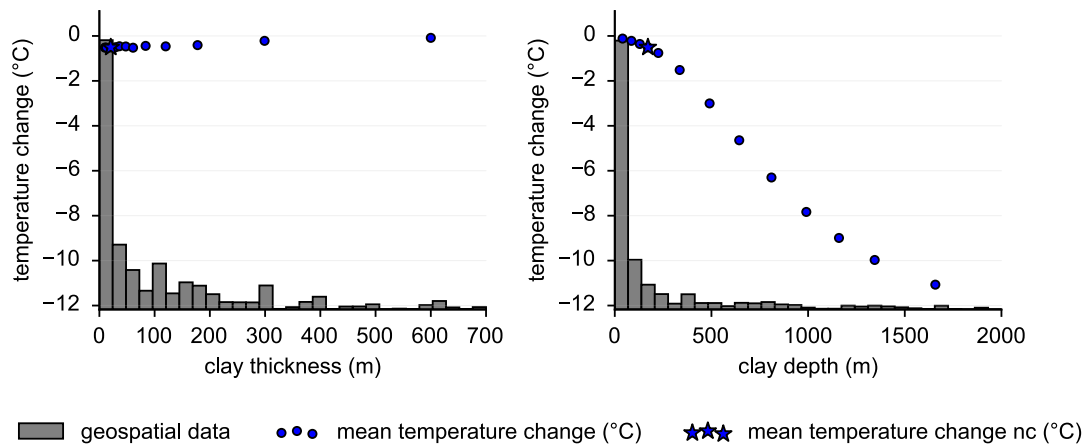


**Figure 19.** Mean temperature change (°C) in comparison to a no-flow scenario as function of clay thickness (right above) and clay depth (left down) with the probability distribution of the respective parameter presented in the histograms.

## **4 Discussion**

The discussion first compares our results to other literature. Next, it elaborates on the limitations of the research and on the implications of the study's outcomes.

### **4.1 Results literature comparison**

Like Kooi (2016), we find that recharge reduces basins temperature by several tens of degrees. In his paper, Kooi refers little to permeability and implies that crustal rocks i.e. crystalline rocks experience more groundwater flow than sediments. This affects hydraulic gradient, as recharge values are predefined. When reconstructing our base case with crystalline rock, recharge equaling the median value of our database (0.07881 m/yr) and defining the recharge-discharge boundary at 5 %, the hydraulic gradient equals approximately 4.3286. This value is unlikely, even for the Himalayas. In our approach head is specified and recharge is allowed to float. Hereby, we achieve more realistic hydraulic gradient values and more likely permeability fluid flow dependencies.

Bjørlykke et al. (1988), demonstrate that low permeability layers of less than 1 m thickness can split one large convection cell into two smaller ones. This is comparable to our findings that clay layers reduce vertical flow velocity to below 1 cm/yr, when between 0.1 mm and 100 m thick, depending on the clay type.

### **4.2 Limitations and implications**

Based on the results of our compiled dataset, shale layer thickness in reality always blocks fluid flow by reducing vertical flow velocity in the clay layer to below 1 cm/yr. This can be explained by the lack of thin clay layers in the database, seeing thinner clay layers are permeable as concluded in chapter 3.3.1. The absence of thin shale zones in our dataset might not be realistic.

Potentially, they were neglected in the stratigraphy. Future databases, compiling the global distribution on thin clay layers might provide more clarity on the matter.

Also, our simulation assumes the clay layers to be continuous. As we only compiled data from marine clay layers this might be relatively realistic. Nevertheless, faults are seldom absent. Faults will most likely increase permeability, thereby leaving our reconstructed flow velocity and temperature change to be distorted, i.e. too small. Incorporating realistic fault distributions into the scenario, would increase accuracy and therefore be interesting for future research.

Furthermore, in our results vertical flow velocity in the clay layer is higher with increasing basin dimensions. However, we find that velocity declines with greater basin dimensions in the equivalent scenario without clay layer. This result is counter-intuitive and so far we have no explanation for this outcome.

Moreover, the results show permeability values of  $1e^{-13}$  m<sup>2</sup> or less in the coarse grained areas. These values are lower than expected from Gleeson et al. (2011). The low permeability values might indicate potential room for improvement.

Besides that, our model does not take density variations into account and neglects the effect of salinity. These factors are likely to influence both fluid and heat flow. Therefore, incorporating dependencies can increase the accuracy of outcomes.

We also expect the results to be somewhat distorted due to the resolution we used. Therefore, more accurate outcomes may be expected when increasing the grid size, which for this study equals 200 cells in the x direction and 150 in the y direction.

As mentioned in the introduction, the results might find application in fields related to geothermal energy and nuclear waste repositories. Alternative geothermal gradients yield several insights on for instance regional solute transport or hydrocarbon reserves. As clay layers have shown to influence heat flow, further research integrating the effect of shale on such systems could create further insights on for instance arsenic contamination in aquifers.

## 5 Conclusion

In sum, we conclude from our new database that marine shale layers are present in all of North America and roughly 40% of the research area in Europe. Most clay layers are roughly 20 m thick and buried 170 m deep.

Base case scenario results show that a shale layer reduces vertical fluid flow to below 1 cm/yr and decreases the cooling effect of recharge by up to 20 °C.

The flow velocity and temperature deviation due to the presence of a clay layer increases with increasing hydraulic gradient and declining clay content of the sediment surrounding the clay layer. As dimensions of a clay layer free basin increase, velocity decreases. Velocity approaches 0 m/yr for sediments with a 20 m thick clay layer regardless of the dimensions, which also applies to temperature change. Temperature change has a maximum around 50 km half-length for clay layer free watersheds.

If a clay layer is present, vertical flow velocity increases in and above the shale zone and declines below it with increasing basin size. Velocity increases all three zones with higher hydraulic gradients and decreases in the respective zones with increasing clay content of the surrounding sediment.

In our dataset, almost all clay layers reduce the vertical flow velocity in the clay layer to below 1 cm/yr. Thus, the majority of clay layers in our database act as non-permeable barriers to fluid and heat flow. We find that continuous kaolinite, illite and smectite layers of 10 – 100 m, 1-10 cm and 0.1-1.0 mm thick respectively, block groundwater flow.

As clay zone burial deepens and as clay zones become thicker vertical flow velocity declines in and below the shale layer and increases above it. The deviation between velocities in different layers, which is also mentioned

before, does not occur for temperature, which either increases or decreases in all layers. We find that the suppression of the heat flow decreases with clay layers burial depth, allowing a cooling effect up to  $-11\text{ }^{\circ}\text{C}$ .

## 6 Acknowledgement

First and foremost, I would like to thank my chief supervisor Elco Luijendijk. Your inexhaustible patience, curiosity and humor have been a great source of energy over the last months. Besides introducing me to your areas of expertise, you also integrated me socially into the department. You never cease to think along e.g. send related or just interesting papers, even whilst planning world domination and academic fame. I count myself lucky to have had so much fun over the course of my bachelor thesis. Moreover, you gave me the opportunity to gain insight into how a career as a researcher at university might look like.

Also, I would like to express my gratitude towards second supervisor Tom Gleeson. Thank you for lending me your brains to pick multiple times in the last couple of months. I appreciate how you always find time to review results, and more importantly to question them.

Most of all, I would like to thank both of you for the positive environment you create. I feel you encourage me to stay with my head in the clouds whilst leaving my feet on the ground. This enabled and provoked me to pursue ambitious goals and to achieve steady results. I value the vast amounts of knowledge that you both have and how you welcomed me to be involved in the development of your brainchild. Over the last month, I felt nothing but socially, intellectually and pedagogically pampered. I enjoyed working with you both and consider the future students that may call you their supervisors privileged.

Furthermore, I would like to thank TNO for the supporting data.

## 7 Literature

Allen, P.A., Allen, J.R. (2005) *Basin Analysis* - 2nd ed. Blackwell Publishing, Oxford, UK.

Anderson, M. P. (2005), *Heat as a Ground Water Tracer*, *Ground Water*, 43(6), 951-968.

Athy, L. F. (1930), *Density, porosity and compaction of sedimentary rocks*, *AAPG Bulletin*, 14(1), 1-24.

Barbier, E. (2002), *Geothermal energy technology and current status: an overview*, *Renewable and Sustainable Energy Reviews*, 6, 3-65.

Bjørlykke, K., Mo, A., Palm, E. (1988), *Modelling of thermal convection in sedimentary basins and its relevance to diagenetic reactions*, *Marine and Petroleum Geology*, 5(4), 338-351.

Carman, P. C. (1937) *Fluid flow through granular beds*, *Transactions, Institution of Chemical Engineering*, London, 15, 150 – 160.

Carman, P. C. (1956) *Flow of gases through porous media*. Butterworths, London.

Chapuis, R. P., Aubertin, A. (2003), *On the use of the Kozeny-Carman equation to predict the hydraulic conductivity of soils*, *Canadian Geotechnical Journal*, 628(1927), 616-628.

Corbet, T. F., Bethke, C. M. (1992), *Disequilibrium Fluid Pressure and Groundwater Flow in the Western Canada Sedimentary Basin*, *Journal of Geophysical Research*, 97(B5), 7203-7217.

- Darcy, H. (1856). *Les Fontaines Publiques de la Ville de Dijon*
- Davies, J. H. (2013), *Global map of solid Earth surface heat flow*, G3, Volume 14, Issue 10, 4608-4622.
- Deming, D. (1994), Fluid flow and transport in the upper continental crust, Geological Society London, Special Publications, 78(1), 27-42.
- Doornenbal, H., Stevenson, A. (2010) *Petroleum Geological Atlas of the Southern Permian Basin Area*, Houten, The Netherlands, EAGE.
- Fourier, J. B. J. (1822) *Théorie analytique de la chaleur*. Paris.
- Fowler, A. C., Yang, X. S. (1998), *Fast and slow compaction in sedimentary basins*, SIAM Journal on Applied Mathematics, 59(1), 365-385.
- Gleeson, T., Smith, L., Moosdorf, N., Hartmann, J. Dürr, H. H., Manning, A. H., van Beek, L. P. H., Jellinek, A. M. (2011) *Mapping permeability over the surface of the Earth*, Geophysical research letters, vol. 38, Iss. 2, doi: 10.1029/2010GL045565
- Gleeson, T., Befus, K. M., Jasechko, S., Luijendijk, L., Cardenas, M. B. (2016) *The global volume and distribution of modern groundwater*, Nature Geoscience, Vol. 9, 161-167.
- Hansen, J., Ruedy, R., Glascoe, J., Sato, M. (1999) *GISS analysis of surface temperature change*, *Journal of Geophysical Research, Atmospheres*, Vol. 104, No. D24, pp. 30997-31022.
- Hendry, J. (2015), *Can argillaceous formations isolate nuclear waste? Insights from isotopic, noble gas, and geochemical profiles*, *Geofluids*, 15, 381-186.

- Holdich, T. G. (2002), *Fundamental of partible technology*, Midland Information Technology; Publishing, Loughborough.
- Klemme, H. D. (1972) *Geothermal gradients Part 2 Heat influences size of oil giants*, Oil and Gas Journal, Volume 70, 30.
- Kooi, H. (2015), *Groundwater flow as a cooling agent of the continental lithosphere*, Nature Geoscience, 9, 227-230.
- Kozeny, J. (1927) *Ueber kapillare Leitung des Wassers im Boden*, Sitzungsver Akad. Wiss., Wien, 136 (2a), 271-306.
- Lehner, B., Verdin, K., Jarvis, A. (2006) *HydroSHEDS Technical Documentation*, World Wildlife Fund, Washington, DC.
- Luijkendijk, E. (2012) *The role of fluid flow in the thermal history of sedimentary basins*, Vrije Universiteit van Amsterdam.
- Luijkendijk, E., Gleeson, T. (2015), *How well can we predict permeability in sedimentary basins? Deriving and evaluating porosity-permeability equations for noncemented sand and clay mixtures*, Geofluids 15, 67-83.
- Makrostrat, [www.macrostrat.org](http://www.macrostrat.org)
- Mavko, G. Nur, A. (1997), *the effect of a percolation threshold in the Kozeny-Carman relation*, Geophysics, 62(5), 1480-1482.
- Mavko, G., Mukerji, T. and Dvorkin, J. (2009), *The rock physics handbook: Tools for seismic analysis of porous media*, Cambridge university press.

Neuzil, C. (1994), *How permeable are clays and shales?*, Water Resources Research, 30(2), 145-150.

Ranjram, M., Gleeson, T., Luijendijk, E. (2015) *Is the permeability of crystalline rock in the shallow crust related to depth, lithology or tectonic setting?* Geofluids, 15, 106-119.

Revil, A., Cathles, L. M, (1999), *Permeability of Shaly Sands*, Water Resources Research, 35(5), 651-662.

Vos, C. I., Prevost, A. M. (2010) *SUTRA: A model for saturated-unsaturated variable-density ground-water flow with solute or energy transport*, water-resources investigations report 02-4231, USGS.

## 8 Appendix

### Appendix A

#### Equations for fluid and heat flow

Fluid flow, heat flow and all related parameters are determined using a customized version of SUTRA. The central equations for regional fluid and heat flow are based on Darcy's law and Fourier's law on thermal conduction.

#### 1.1 Fluid flow

As mentioned above fluid flow is assumed to follow Darcy's law. As the model operates under steady state conditions it is implied that:

$$-\nabla q + W = 0 \quad (1)$$

This is the simplest form of Darcy's law where  $q$  is fluid flux (m/s),  $W$  is a source term ( $s^{-1}$ ). Darcy flux  $q$  is the function of hydraulic conductivity ( $k$ ) and the hydraulic head ( $h$ ). As  $k$  is a function of fluid density ( $\rho$ ), gravitational acceleration ( $g$ ), viscosity ( $\mu$ ), the Darcy flux may be expressed as:

$$q = -\left(\frac{k\rho g}{\mu}\right)\nabla h \quad (2)$$

where, hydraulic head ( $h$ ) is a function of pressure ( $p$ ), fluid density ( $\rho$ ), gravitational acceleration ( $g$ ) and height ( $z$ ):

$$h = p + \rho g \quad (3)$$

When integrating the latter two equations in to the main flow equation, fluid flow is assumed to follow:

$$-\nabla\left(-\frac{k\rho g}{\mu}\right)\nabla(p+\rho g z)+W=0 \quad (4)$$

Thus, in sum fluid flow is a function of fluid density ( $\rho$ ), fluid viscosity ( $\mu$ ), permeability ( $k$ ), pressure ( $p$ ) and gravitational acceleration ( $g$ ). The latter is assumed to be  $9,81 \text{ ms}^{-2}$ . All further parameters mentioned are discussed in the following paragraphs 2.1.2 to 2.1.4, followed by the heat flow equations in 2.1.5.

## 1.2 Fluid viscosity and density

For energy transport viscosity ( $\mu$ ) is considered to be a function of temperature ( $T$ ) (Voss & Provost, 2010):

$$\mu = \mu(T) \cong (239.4 * 10^{-7}) 10^{\left(\frac{248.37}{T+133.15}\right)} \quad (5)$$

Also, fluid density ( $\rho$ ) is assumed a function of temperature for energy transport (Voss, C. I., Provost, A. M., 2010):

$$\rho = \rho(T) \cong \rho_0 + (T - T_0)\left(\frac{\delta\rho}{\delta T}\right) \quad (6)$$

where  $\rho_0$  equals the base fluid density at  $T=T_0$  and  $T_0$  is the base fluid temperature.

## 1.3 Permeability

The permeability of sand and silt was calculated using the Kozeny-Carman equation (Kozeny, 1927; Carman, 1937; Carman, 1956).

$$k_{sd} = \frac{1}{cS_s^2} \frac{\phi^3}{(1-\phi)^2} \quad (7)$$

where  $\phi$  is the porosity,  $S_s$  ( $m^{-1}$ ) is the specific surface of sand and  $C$  is the Kozeny-Carman constant. Porosity has no dimension. The equation was slightly adjusted by using effective porosity ( $\phi_e$ ) instead of total porosity ( $\phi$ ) (Mavko et al., 1997):

$$\phi_e = \phi - \phi_t \quad (8)$$

where  $\phi_t$ , the percolation threshold, was assumed 2% (Mavko et al., 2009).

Specific surface ( $S_s$ ) was calculated in accordance with Holdich (2002) and Chapuis and Aubertin (2003):

$$S_s = 6.0 \sum \frac{f}{D} (1 - \phi) \quad (10)$$

where  $D$  is the grain size (m) and  $f$  is the mass fraction of the grain size. Also, here total porosity ( $\phi$ ) is used, not effective porosity ( $\phi_e$ ).

Grain size distribution was assumed to be a function of clay content, following Luijendijk and Gleeson (2015):

$$\sigma^2 = 2.39w + 1.18 \quad (11)$$

Clay permeability was determined using an empirical permeability-void ratio formula from Luijendijk and Gleeson (2015):

$$k_{cl} = k_0 v^m \quad (12)$$

where  $k_{cl}$  is the permeability of the clay components and  $k_0$  is the reference permeability. Kaolinite, illite and smectite were ascribed  $k_0$  values of  $6.16e-17$   $m^2$ ,  $1.54e-19$   $m^2$  and  $1.18e-21$   $m^2$ , respectively. Parameter  $v$  is the void ratio and  $m$  an empirical parameter for kaolinite, illite or smectite. These are assumed 3.61, 3.58 and 3.01, respectively. The void ratio equals:

$$v = \frac{\phi}{1-\phi} \quad (13)$$

Permeability values of sediments that were a mixture of sand, silt and clay were determined by calculating the power mean of the permeability of sand or silt (eq. 7- 11) and clay (eq. 12 and 13):

$$k = (wk_{cl}^p + (1-w)k_{sd}^p)^{\frac{1}{p}} \quad (14)$$

In this formula  $w$  represents the fraction of clay,  $p$  the power mean coefficient,  $k_{cl}$  the clay element and  $k_{sd}$  the sand and silt element. The power mean coefficient ( $p$ ) was assumed to be 0.

Permeability that is direction-independent is called isotropic. When the permeability does depend on the direction it is considered anisotropic. All previous equations apply to horizontal permeability. The vertical permeability is lower, which is reflected in the anisotropy factor. The anisotropy depends on scale. When applying it on basin scale the anisotropy is a consequence of alternating permeable and less permeable layers. This is represented in the model by the placement of the clay layer. Therefore, we require the anisotropy scaled to one model grid cell. As this will probably be higher than the reference value in Gleeson & Lujendijk (2015), the value is assumed 10.

All the aforementioned, regarding permeability concerns non-cemented sediments. Thereby, it applies to the upper 2km of the 3km deep simulation. Cemented sediments were ignored in this section, because significant diagenesis starts around 80 °C, i.e. 2 to 3 kilometers depth (Lujendijk et al., 2015). Exceptions arise with high calcite fraction, as it mobilizes in lower temperatures. A second exception regards basins that have undergone exhumation, in which sediments have been buried at greater depths in the past. In this basement section i.e. the lowest kilometer, sediments are

governed by a crystalline rock permeability depth function from Ranjram et al. (2015):

$$k = K \left( \frac{\mu}{\rho g} \right) \quad (15)$$

where,  $k$  is permeability ( $m^2$ ),  $K$  hydraulic conductivity ( $m/s$ ),  $\mu$  viscosity ( $pa-s$ ),  $\rho$  density ( $kg/m^3$ ) and  $g$  the gravitational acceleration which is assumed to equal  $9.81 m/s^2$ .

#### 1.4 Porosity

Furthermore, a porosity depth dependency was integrated into the model, based on Anthy (1930), Bond and Kominz (1984), Sclater and Christie (1980) and Luijendijk (2012):

$$\phi = \phi_0 e^{-cz} \quad (16)$$

where  $\phi_0$  is the porosity at the surface,  $z$  the depth ( $m$ ) and  $c$  a porosity-depth parameter ( $m^{-1}$ ), which varies between  $4 \times 10^{-4}$  and  $9 \times 10^{-4} m^{-1}$  for clay and sand respectively (Luijendijk, 2012).

#### 1.5 Heat Flow

The simplest steady state version of thermal conduction is analogue to Darcy's law on steady state fluid flow:

$$\nabla q_w + W_t = 0 \quad (17)$$

Where  $W_t$  is the heat production ( $s^{-1}$ ), and  $q_w$  is a function of thermal conductivity ( $K_t$ ) and temperature ( $T$ ) (Fourier, 1822):

$$q_w = K_t \nabla T \quad (18)$$

The thermal conductivity was assumed  $2.5 \text{ Wm}^{-1}\text{K}^{-1}$  and  $0.6 \text{ Wm}^{-1}\text{K}^{-1}$ , for solids and fluids respectively. Besides thermal conduction, advection causes heat flow. Advection is described by:

$$\rho_f c_f \vec{q}_f \quad (19)$$

Where  $\rho_f$  is the fluid density,  $c_f$  the and  $q_f$  the Darcy flow.

Together equations 17, 18 and 19 describe all significant heat transport as:

$$K_t \nabla T + \rho_f c_f \vec{q}_f + W_t = 0 \quad (20)$$

## **Appendix B – E**

Please find the appendix B, C, D and E on the CD-ROM attached to the last page of the booklet.

## **Declaration of Authorship**

I do solemnly declare that I, Virginia Attje Ingrid Albertine Potter van Loon, have written the presented bachelor thesis with the title: “How clay layers control basin-scale fluid and heat flow” by myself without undue help from a second person, others and without using such tools other than that specified. Where I have used thoughts from external sources, directly or indirectly, published or unpublished, this is always clearly attributed. I am aware that a false statement will have legal implications.

Göttingen, Germany, 16 June 2016

---